Int. J. Heat Mass Transfer. Vol. 24, No. 11, pp. 1771–1782, 1981
Printed in Great Britain

0017–9310/81/111771–12 $02.00/0
Pergamon Press Ltd.

HEAT AND MASS TRANSFER IN AN EMITTING COMPRESSED LAYER WITH REFLECTION FROM THE BODY SURFACE AND INJECTION OF ABLATION PRODUCTS

M. N. ROLIN, R. I. SOLOUKHIN and F. B. YUREVICH
Heat and Mass Transfer Institute, Minsk, U.S.S.R.

(*Received* 29 *August* 1980)

Abstract—The paper is concerned with the analysis of radiative–convective heat transfer of an axisymmetric blunt body in a hypersonic air flow. The results of calculation of radiative and convective heat fluxes to the ablating graphite surface are presented. The effect of allowance for radiation transfer on the predicted radiative heat flux is shown.

A quantitative assessment is made of the tendency of heat fluxes directed to a reflecting surface to increase due to absorption of reflected radiation in a compressed layer.

NOMENCLATURE

B_ν, Planck function;
D_{ij}, binary diffusion coefficient of components i and j;
e, electron charge, electron index;
G_w, mass flow rate of blowing through body surface;
J_j, diffusional mass flux of the chemical component j of gas mixture;
H, gas enthalpy;
H_i, specific enthalpy of component i;
H_0, enthalpy of coating material in the initial state;
k, Boltzmann constant;
k_ν, optical absorption coefficient;
m_i, molecular mass of component i;
N_j, volumetric density of j component particles;
p, gas pressure;
p_k^{sat}, p_k, saturated vapour pressure of the kth species and its partial pressure, respectively;
r, reflectivity;
R, blunt body radius; universal gas constant;
q_c, convective heat flux;
q_r, integral radiative heat flux;
q_ν^r, spectral radiative heat flux;
$q^{r\pm}$, radiative heat flux components: (+) positive and (−) negative directions along the y-axis;
u, v, longitudinal and transverse gas velocities;
V_∞, incident flow velocity;
x, y, longitudinal and transverse coordinates of compressed layer;
x_i, mole fraction of component i in gas mixture;
α_k, mass fraction of kth species in gas mixture; accommodation coefficient in the Langmuir–Knudsen zone for kth species;
γ_{kj}, mass fraction of kth species in chemical component j of gas mixture;
ν, frequency (wavenumber) of radiation;
σ_ν, optical absorption cross-section;
z_i, multiplicity of the charge of component i particles;
ρ, μ, λ, density, viscosity and thermal conductivity of gas, respectively.

Subscripts

s, conditions right behind the shock;
w, conditions on the surface;
∞, conditions in incident flow;
o, conditions deep in the material.

INTRODUCTION

THE SURFACE of space vehicles that re-enter the Earth's atmosphere, or enter the atmospheres of other planets, is exposed to thermal radiation from a compressed and shock-heated gas layer. Since emission of radiation is coupled with gas-dynamic processes, heat conduction and diffusion effects, the heat transport under these conditions is referred to as radiative–convective heat transfer in hypersonic flow. Strong radiative–convective heating may bring about decompositions of the body heat shield attended by blowing of the ablation gas products into the compressed layer. The blowing, in its turn, can have an effect on radiative and convective heat fluxes to the surface. A reduction in this heating can be achieved by the use of highly reflective coatings. But an important face here is that the reflected radiation can be absorbed in the compressed layer thus increasing its temperature. As a consequence, radiative–convective heat fluxes to a reflect-

ing surface can exceed those directed to the surface which completely absorbs the incident radiation.

A quantitative evaluation of the effect exerted by ablation products and radiation reflected from the surface on radiative–convective heat transfer characteristics is essential for the design of systems which can provide reliable thermal protection against aerodynamic heating at hypersonic velocities.

Experimental simulation of radiative–convective heat transfer conditions is found to be difficult because of the requirement for reproducibility of actual geometric dimensions which is bound with large energy expenditures. At present, theoretical studies provide the major source of information on radiative–convective heat transfer. These are based on numerical modelling of the process with the use of electronic computers.

The present situation with regard to the study of radiative–convective heat transfer at hypersonic velocities can be inferred from [1–7]. Paper [1] presents the results of calculations of radiative–convective heat transfer of a blunt impermeable-surface body in a hypersonic flow. Besides continuum contribution, these calculations allow for the line contributions of atoms and ions—an operation which presents great computing difficulties. The importance of line transport for the radiative heat transfer in a compressed layer is shown. This effect has also been accounted for in calculations of radiative heat transfer in flows behind shock waves presented in [2].

Detailed studies of the effect of blowing of graphite ablation products on heat transfer have been carried out in [3, 4], but the calculations presented were made without regard for the line transport. In addition, most of these has been carried out on the assumption of no chemical reactions, i.e. in the "frozen" boundary layer approximation, and only a few, on the assumption of chemical equilibrium in the boundary layer.

A simultaneous account for the blowing of ablation products and line transport was made in [5–7]. In [5], a wide range of flow conditions is considered, but the compressed layer is assumed to be inviscid and non-conductive. Air and ablation products are assumed to be separated by a discontinuity surface. In [6, 7], both viscosity and thermal conductivity effects have been taken into consideration, but the body of data on heat transfer under different flow conditions is insufficient.

Radiative–convective heat transfer in hypersonic flow is generally calculated with the aid of simplified diffusion models. In [5, 6], diffusion of ablation products has not been accounted for at all. The authors of [3, 4] have employed the model of binary diffusion. An attempt to allow for a multi-component diffusion has been made in [7], but here ionization of the compressed layer has been ignored.

A quantitative evaluation of the effect of radiation reflected from the surface and absorbed in the compressed layer was made only in [8], where an impermeable surface with the reflection coefficient independent of frequency was considered.

In the present work calculations have been made of radiative–convective heat transfer on a permeable surface weth regard for both the line transport and behaviour of collisional transfer due to ionization in the compressed layer and multi-component nature of diffusion. The extent of calculations is sufficient for establishing the effect of variations in the independent parameters of the problem, such as velocity of flight, pressure in the compressed layer and body dimensions, on radiative–convective heat transfer for permeable and impermeable reflecting surfaces. Here, both the surfaces with ideal optical properties and made of actual material (tungsten, silicon) are considered. The ambient medium is air and the ablative material is graphite the choice of which has been dictated by its efficiency as a heat shield and by a sufficient body of data available on the optical properties of its ablation products. A model problem of heat transfer on the surface with ideal reflecting properties, through which the graphite ablation products are injected, is also considered.

PHYSICAL SCHEME OF PROCESSES OCCURRING IN A COMPRESSIBLE LAYER. GOVERNING EQUATIONS AND PREDICTION METHODS

Since minute details of physical processes occurring in a compressed layer will be accounted for in what follows, it would be advisable to limit consideration by the vicinity of the stagnation point of an axisymmetric blunt body. This enables one to simplify the mathematical description of the problem and carry out calculations with the quantity of versions sufficient for the results to be analyzed.

A hypothetical local thermodynamic equilibrium in the compressed layer is adopted. The validity of this is discussed elsewhere [1].

The flow in the vicinity of the stagnation line is described with the aid of asymptotic approximations to the Navier–Stokes equations for high Mach and Reynolds numbers [6, 8]. In the coordinate system shown in Fig. 1 the set of conservation equations is:

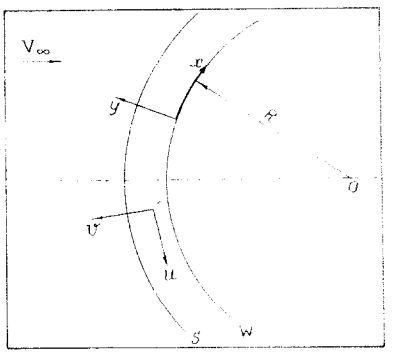

FIG. 1.

continuity

$$2\rho\left(\frac{\partial u}{\partial x}\right)+\frac{\partial}{\partial y}(\rho v)=0, \tag{1}$$

momentum

$$\rho\left(\frac{\partial u}{\partial x}\right)^2+\rho v\frac{\partial}{\partial y}\left(\frac{\partial u}{\partial x}\right) = -\frac{\partial^2 p}{\partial x^2}+\frac{\partial}{\partial y}\left[\mu\frac{\partial}{\partial y}\left(\frac{\partial u}{\partial x}\right)\right], \tag{2}$$

$$\frac{\partial p}{\partial y}=0, \tag{3}$$

energy

$$\rho v\frac{\partial H}{\partial y}=-\frac{\partial}{\partial y}\left(-\lambda\frac{\partial T}{\partial y}+\sum_j J_j H_j+q^r\right), \tag{4}$$

species

$$\rho v\frac{\partial \alpha_k}{\partial y}=-\frac{\partial}{\partial y}\left(\sum_j \gamma_{kj}J_j\right). \tag{5}$$

In equations (4) and (5), summation is performed over all of the gas mixture components which are taken into account, i.e. atoms, ions, molecules, free electrons inclusive. The subscript k in (5) refers to the chemical elements present in the mixture, i.e. nitrogen, oxygen, carbon. The quantity $(\partial u/\partial x)$ is considered to be a function of the coordinate y.

The boundary conditions at the shock derive from the generalized Rankin–Hugoniot relations [8]:

$$\rho_\infty V_\infty = -\rho_s V_s,$$

$$\rho_\infty V_\infty\left[\frac{V_\infty}{R}-\left(\frac{\partial u}{\partial x}\right)_s\right]=\left[\mu\frac{\partial}{\partial y}\left(\frac{\partial u}{\partial x}\right)\right]_s,$$

$$\rho_\infty V_\infty^2\left(H_\infty+\frac{V_\infty^2}{2}-H_s\right)=-\left(-\lambda\frac{\partial T}{\partial y}+\sum_j H_j J_j\right)_s,$$

$$\rho_\infty V_\infty(\alpha_{k\infty}-\alpha_{ks})=-\left(\sum_j \gamma_{kj}J_j\right)_s,$$

$$p_s=p_\infty+\rho_\infty V_\infty^2\left(1-\frac{\rho_\infty}{\rho_s}\right). \tag{6}$$

The gas in the incident flow is assumed to be non-absorbing, i.e. cold. At the surface we assign the conditions of zero velocity, mass flux continuity, equal gas and wall temperatures and mass balance of species:

$$\left(\frac{\partial u}{\partial x}\right)_w=0,\quad \rho_w V_w=G_w,\quad T_w=T'_w,$$

$$\rho_w V_w\alpha_{kw}-G_w\alpha_{ko}=-\left(\sum_j \gamma_{kj}J_j\right)_w, \tag{7}$$

where α_{ko} is the mass fraction of the kth species in the injected gas, T'_w is the wall temperature.

Closure of equations (1–5) is achieved through the formula for the pressure gradient derived from modified Newton's theory [9]

$$\frac{\partial^2 p}{\partial x^2}=-\frac{8}{3}\rho_\infty\frac{V_\infty^2}{R^2}.$$

The radiative heat flux is calculated in the approximation of a locally one-dimensional infinite planar layer [1]. The optical properties of the surface are assumed to be isotropic, i.e. independent of direction. The cases of specular and diffuse reflection are considered. In conformity with this

$$q^r=\int_0^\infty q_\nu^r\cdot d\nu,$$

$$q_\nu^r(\tau)=2\pi\int_0^{\tau_s} B_\nu(\tau')E_2(|\tau-\tau'|)\times \operatorname{sign}(\tau-\tau')\,d\tau'+\Delta q_{\nu w}^r(\tau), \tag{8}$$

where $\Delta q_{\nu w}^r$ is the radiative flux component due to reflection and emission from the surface, τ is the optical thickness reckoned from the surface which is

$$\tau=\int_0^y k_\nu(y)\,dy.$$

For the surface with diffuse and specular reflection we have respectively

$$\Delta q_{\nu w}^{\text{diff}}=2\pi(1-r_\nu)B_{\nu w}E_3(\tau)+2\pi r_\nu E_3(\tau)\int_0^{\tau_s}B_\nu(\tau')E_2(\tau')\,d\tau',$$

$$\Delta q_{\nu w}^{\text{spec}}=2\pi(1-r_\nu)B_{\nu w}E_3(\tau)+2\pi r_\nu\int_0^{\tau_s}B_\nu(\tau')E_2(\tau+\tau')\,d\tau'. \tag{9}$$

Formulae (8) and (9) contain integro-exponential functions defined by

$$E_n(\tau)=\int_1^\infty\frac{e^{-\tau p}}{p^n}\,dp.$$

The absorption coefficient is determined by the formula

$$k_\nu=\sum_j N_j(\sigma_{\nu j}^1+\sigma_{\nu j}^2\cdot N_e),$$

the summation in which is carried out over all of the mixture components taken into account, with the exception of electrons. The absorption cross-section $\sigma_{\nu j}^1$ refers to bound–bound and bound–free transitions in the field of a given particle. The calculation technique for radiative heat fluxes is described in [12]. The gaseous medium of the compressed layer injected by graphite ablation products was assumed to involve the following components:

N_2, O_2, NO, C_2, CO, CN, C_3, CO_2, N, O, C, NO^+, CO^+, N^+, O^+, C^+, N^-, O^-, C^-, e.

The coefficients of optical absorption were determined with the use of the absorption cross-sections for air components borrowed from [10], the absorp-

tion cross-sections for graphite ablation products, from [11, 13]. The lacking cross-sections for photoionization of molecular graphite ablation products were adopted in the same manner as in [3–5]. An additional account was made of the C_2 molecule fringes, the absorption cross-sections for which were taken from [14]. The fringes of C_3 at $\nu = (20–50) \cdot 20^3\ \text{cm}^{-1}$ were taken into account following the model suggested in [15]. When carrying out calculations, the entire spectral range $\nu = (10–2 \cdot 10^5)\ \text{cm}^{-1}$ was partitioned into 96 parts in each of which the continuum contribution absorption coefficients were replaced by the averaged ones. One hundred and forty strong multiplets of atoms and ions of nitrogen, oxygen and carbon were taken into account separately. These comprised the first items of band sequences. The occurrence of a great number of weak spectral lines of band sequences coming to photoionization thresholds of the energy states associated with the basic electronic configuration of atoms were taken into account with the aid of the band model [12]. For the excited electronic configurations a shift in photoionization thresholds was introduced according to [10].

The diffusion fluxes were determined from the Stefan–Maxwell equations written out with account for ionization in the compressed layer [16]

$$\frac{m}{\rho}\sum_j \frac{1}{D_{ij}}\left(\frac{x_i J_j}{m_j} - \frac{x_j J_i}{m_i}\right) = \frac{\partial}{\partial y} x_i - x_i \frac{eE}{kT} z_i, \tag{10}$$

$$\sum_j J_j = 0, \tag{11}$$

where E is the strength of the electric field induced by diffusive separation of charges. Summation in these formulae is carried out over all of the gas mixture components taken into account. As shown in [16], the gas in the compressed layer can be considered to be a quasi-neutral one which engenders

$$\sum_j x_j z_j = 0.$$

Moreover, it is assumed that there is no electric current to the wall and thereby, according to [16], over the entire compressed layer. Thus

$$\sum_j \frac{J_j}{m_j} z_j = 0. \tag{12}$$

The system of equations (10–12) is closed with respect to J_j and E. It is solved with the use of an approximate procedure described in [17].

The coefficients λ and μ are calculated following the method described in [18]. The system of conservation equations (1–7) is solved numerically [19].

For checking the results, calculations of radiative-convective heat transfer on an impermeable surface have been carried out under the conditions for which the data are available in literature. The comparison between the predicted and reported values of q_w^{r-} is given in Table 1. The agreement observed can be regarded as good.

EFFECT OF BLOWING OF GRAPHITE ABLATION PRODUCTS ON HEAT TRANSFER. ABLATION PARAMETERS

Under the conditions of strong heating, ablation of graphite is dominated by sublimation [20]. We assume that C, C_2, C_3 are the products of evaporation. The rate of decomposition is controlled by the evaporation kinetics, i.e. by the Langmuir–Knudsen law

$$G_w = \sum_k \frac{\varkappa_k(p_{kw}^{sat} - p_{kw})}{\sqrt{2\pi R T_w / m_k}}. \tag{13}$$

Here summation is carried out over the evaporation products.

This equation relates the surface temperature and concentration of species on it to the evaporation rate. The concentration of species is determined by both the surface temperature and the mass transfer processes in the compressed layer and therefore is the function of G_w. The temperature of the body surface, on the other hand, is governed by the heating prehistory and can be considered as an independent parameter. For this temperature to be determined, the problem of internal heat conduction in heat shield should be solved. The input data for its solution are the magnitudes of heat fluxes to the surface. Due to a great variety of possible heating regimes it is more expedient to have an independent solution to the problem of heat transfer in the compressed layer in which the surface temperature or the rate of ablation is specified as a parameter. Then each version may correspond to a certain instant in the process of unsteady-state decomposition. When the flow conditions vary rather slowly with time, a quasi-steady mode of decomposition is established [20]. In this case the condition of heat balance on the body surface is fulfilled

$$q_w^r + q_w^c = G_w(H_w - H_0).$$

This condition can be used to close the system of equations for G_w and T_w.

The calculations have shown that variation of T_w at a fixed G_w has a relatively weak effect on the heat fluxes. On the other hand, the dependence of G_w on T_w is very strong. For this reason it is convenient to use G_w rather than T_w as an independent parameter.

It is practical to represent the results of calculations in the form of the dimensionless parameters

$$\bar{q}^r = \frac{q_w^{r-}}{q_{wo}^{r-}}, \quad \bar{q}^c = \frac{q_w^c}{q_{wo}^c}, \quad f_w = \frac{G_w}{\rho_\infty V_\infty},$$

where q_{wo}^{r-} and q_{wo}^c are heat fluxes to an impermeable surface.

With the object of comparing the results, calculations of heat transfer were carried out without regard for line transport for three versions of the problem given in [4]. The values of $\bar{q}^r$ obtained are given in Table 2.

The coincidence between the results can be considered as satisfactory. The disagreement available can

Table 1. Comparison of the heat transfer calculations

V_∞ (km/s)	p_s (atm)	R (m)	q_w^r (kW/cm²) Present work	q_w^r (kW/cm²) Published data	Reference
12	0.3	1	0.45	0.44	[1]
12	1	1	2.0	2.2	[1]
12	3	1	7.7	8.3	[1]
12	10	1	32.7	29.5	[1]
14	0.3	1	0.92	1.0	[1]
14	1	1	3.9	4.4	[1]
14	3	1	14.1	15.9	[1]
14	10	1	56.3	62.0	[1]
18	0.3	1	1.7	1.6	[1]
18	1	1	6.9	6.5	[1]
15.3	0.6	2.75	3.7	3.6	[6]
15.3	1.0	2.75	6.6	6.4	[6]

Table 2. Comparison between the results of calculation of heat transfer on an ablating graphite surface carried out with account for continuum contribution alone, $p=1$ atm, $R=1$ m

T_s (K)	f_w	$\bar{q}^r$ Present work	$\bar{q}^r$ Data from [4]
12000	0.1	0.83	0.75
18000	0.012	0.79	0.77
	0.1	0.53	0.50

be attributed to the use of different data on optical properties of gases.

Calculations of radiative–convective heat transfer on the surface of an ablating graphite with account for the line transport were carried out over the following ranges of parameters: $V_\infty = (12\text{–}18)$ km/s, $p = (0.3\text{–}10)$ atm, $R = (0.3\text{–}3)$ m.

The heat transfer results obtained for an impermeable surface are listed in Table 3.

Figure 2 shows the dependence of $\bar{q}^r$ on f_w under these conditions. The numbers of the curves correspond to the numbers of the rows in Table 3; the appropriate data for $\bar{q}^c$ are given in Fig. 3. Figure 4 shows the dependence of f_w on the surface temperature. It is seen that in all the cases the injection of ablation products leads to a monotonic reduction of the radiative heat flux to the surface. Under massive blowing conditions $\bar{q}^r$'s approach certain limiting values. These minimum values of $\bar{q}^r$ decrease with an increase in the indicent flow velocity.

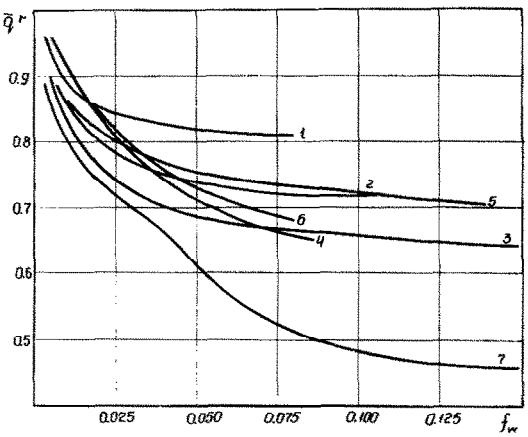

FIG. 2.

Table 3. Specific conditions of flow over a body

No.	V_∞ (km/s)	p (atm)	R (m)	$\rho_\infty V_\infty$ (kg/m²s)	q_{wo}^r (kW/cm²)	q_{wo}^c (kW/cm²)
1	12	1	1	8.88	2.0	1.0
2	15	1	1	6.24	4.7	1.5
3	18	1	1	5.91	6.9	2.1
4	15	1	0.3	6.24	3.2	2.7
5	15	1	3	6.24	6.6	0.81
6	15	0.3	1	2.12	1.1	0.78
7	15	10	1	71.2	66.0	4.5

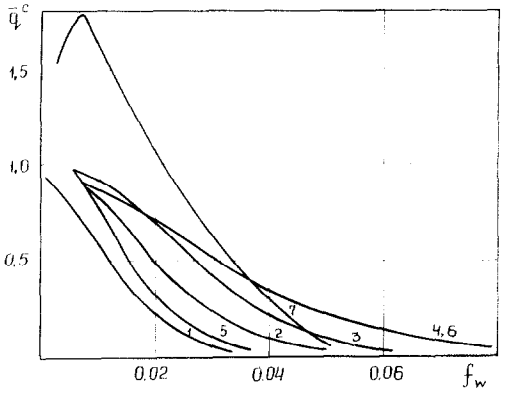

FIG. 3.

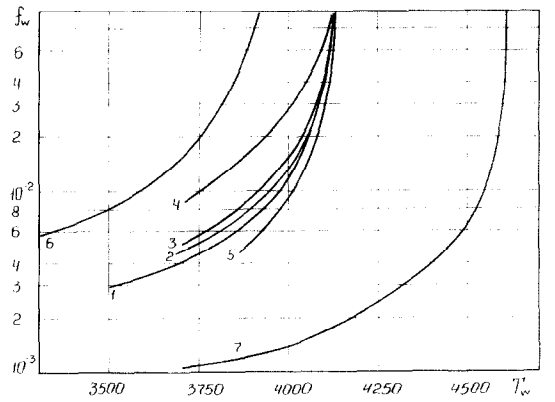

FIG. 4.

When the levels of blowing are high, convective heat fluxes to the surface become blocked completely. At relatively small pressures and body nose radii a monotonic decrease in $\bar{q}_w^c$ is observed with increasing f_w. At large p's or R's in the region of small levels of blowing an increase can occur in the convective heat flux to a permeable surface, as compared with q_{wo}^c. Especially noteworthy is the fact that at equal values of the product $p \cdot R$ the curves of $\bar{q}^c$ vs. f_w are very close and some of them can even merge as is seen in Fig. 3. The mass flow rate of blowing is characterized by a strong dependence on the surface temperature. In this case for each stagnation pressure there is such a temperature at which the plots shown in Fig. 4 have nearly vertical segments. An explanation is that, until the pressure of saturated carbon vapour is less than the pressure in the compressed layer, the partial vapour pressure is close to p_k^{sat} and, according to (13), an increase in the rate of evaporation is small. With the temperature becoming high enough, the vapour pressure attains its limiting value, i.e. p, while p_k^{sat} continues its rapid growth. An increase in the convective heat flux to the surface is observed when $q_w^r \gg q_w^c$.

The appearance of strongly absorbing graphite ablation products in the compressed layer leads to a sharp increase of the temperature gradient in the wall region where thermal conductivity effects are appreciable. This increase in the temperature gradient is not completely balanced out by injection which reduces the convective heat flux [20], since the blowing level is small. As a result, q_w^c becomes larger. It should be noted that in all of the cases the net heat flux to the surface decreases with an increase in the blowing mass flow rate.

Within the whole region of flow conditions studied an increase in q_w^r due to blowing has not been detected, while the authors of [3, 4] observed this effect. The calculations of radiative convective heat transfer, in which a rise in q_w^r showed itself up, were carried out on the assumption of a chemically frozen flow in the layer of ablation products. Because of the high temperature there occurs re-radiation to the surface in the layer of ablation products with its magnitude exceeding that by which the radiative flux from the outer portion of the compressed layer is reduced. In the present work, the reactions in the layer of ablation products were assumed to be at equilibrium. Endothermic reactions of dissociation of C_2 and C_3 substantially decrease the temperature of the layer and weaken re-radiation.

Consider now the effect of the account of line contribution on the predicted radiative heat fluxes to the surface. For this purpose it is convenient to use the parameter, which is equal to the ratio between the radiative heat flux to the surface, obtained with account for the continuum transport alone, and q_w^r, obtained with account for both the continuum and line transport. Denote it by ψ. Figure 5 shows the plot of ψ vs. f_w for the typical flow conditions. It is quite evident that $\psi < 1$. It is particularly noteworthy that this parameter decreases with increasing blowing level which is indicative of the increase in the effect of line contribution on radiative heat transfer with f_w. Thus, the errors in calculations of radiative heating due to a neglect of line transport in the presence of blowing turn to be more substantial than in its absence.

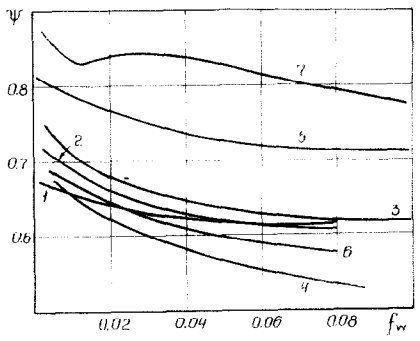

FIG. 5.

In order to clarify the causes for this behaviour of q_w^r let us consider the effect of blowing on separate spectral components. Denote these components by q_{wi}^r, where i is the number of the range. The ranges are selected as follows: (1) $\nu < 10 \cdot 10^3\ \text{cm}^{-1}$; (2) $\nu = (10\text{–}20) \cdot 10^3\ \text{cm}^{-1}$; (c) $\nu = (20\text{–}60) \cdot 10^3\ \text{cm}^{-1}$; (4) $\nu = (60\text{–}87.9) \cdot 10^3\ \text{cm}^{-1}$; (5) $\nu > 87.9 \cdot 10^3\ \text{cm}^{-1}$.

Figure 6 (a, b) shows the dependence of q_{wi}^r on f_w for two versions of flow conditions: (a) $V_\infty = 18$ km/s, $p = 1$ atm, $R = 1$ m; (b) $V_\infty = 15$ km/s, $p = 10$ atm, $R = 1$ m. The solid lines refer to calculations carried out with account for the line transport, while the dash-dotted ones, with account for the continuum contribution alone.

When $p = 1$ atm, reduction in the radiative heat flux to the surface is observed mainly within range 5. Calculations carried out without regard for the line transport show that the radiative flux in this region turns to be high. The explanation of this result lies in the fact that the role of lines within range 5 is small, while extra radiative cooling of the compressed layer due to line transport leads to temperature reduction which is most prominent over the short-wave interval. Range 5 lies within the region of photoionization where the absorption coefficients are large. It is within this region, therefore, that attenuation of the radiative flux to the wall is observed. The absorption coefficients in the remainder ranges turn to be insufficient for causing a decrease in q_{wi}^r. At $p = 10$ atm, radiation in range 5 becomes blocked completely even in the boundary layer on an impermeable surface. In this case blowing causes attenuation of the radiative heat flux mainly in ranges 3 and 4. Attenuation here is approximately proportional to contribution of these ranges into the radiative flux. At the same time, in range 2, where the role of line transport is great, the attenuation due to small absorption coefficients is insignificant. This explains the observed non-monotonic behaviour of the parameter ψ.

The effect of blowing on radiative–convective heat transfer at high pressures has received very little attention in the literature, therefore, it would be worthwhile to consider it in more detail. Figure 7 shows spectral distributions of radiative flux to the surface for $V_\infty = 15$ km/s, $p = 10$ atm, $R = 1$ m. Broken line 1 refers to $f_w = 0$, line 2, to $f_w = 0.08$. In graphing the curves, the line contribution was accounted for in those portions of the spectrum within which they fell on subdividing the latter. It is seen that attenuation occurs mainly at $\nu = (18\text{–}50) \cdot 10^3$ cm and $\nu > 60 \cdot 10^3\ \text{cm}^{-1}$ due, in the first case, to electronic-vibrational bands of molecules C_2 and C_3 and, in the second, to photoionization of the ground and excited states of the basic electronic configuration of the C atom. Figure 8 (a, b) shows the profiles of the spectral components of radiative flux to the surface (a) and the profiles of temperature, enthalpy and molar fractions of components across the compressed layer. As a coordinate which stretches the picture in the wall region we use

$$\eta = \int_0^y \rho\, dy' \Big/ \int_0^{y_s} \rho\, dy'.$$

To increase clarity, Fig. 8(b) shows the dependence of y on η. In this case $y_s = 4.5$ cm, $H_s = 112.5$ MJ/kg $T_s = 17\,200$ K. Figure 8(a) depicts the spatial region in which attenuation of radiative fluxes occurs. It should be noted that appreciable absorption in zone 4 occurs in the region of the mixing layer despite its shortness.

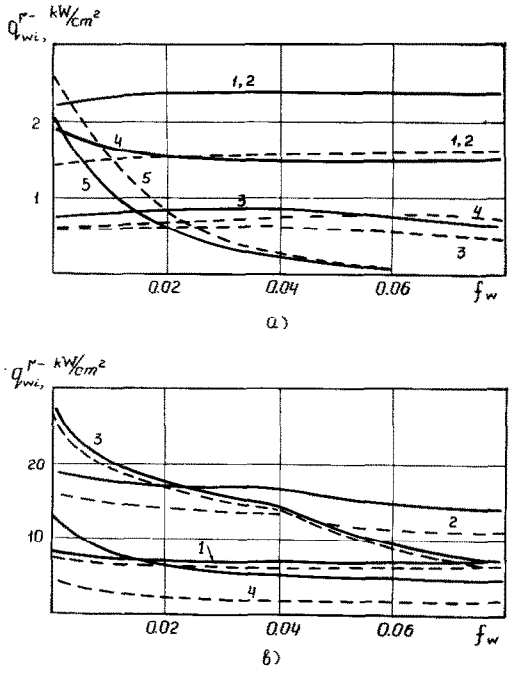

FIG. 6(a, b).

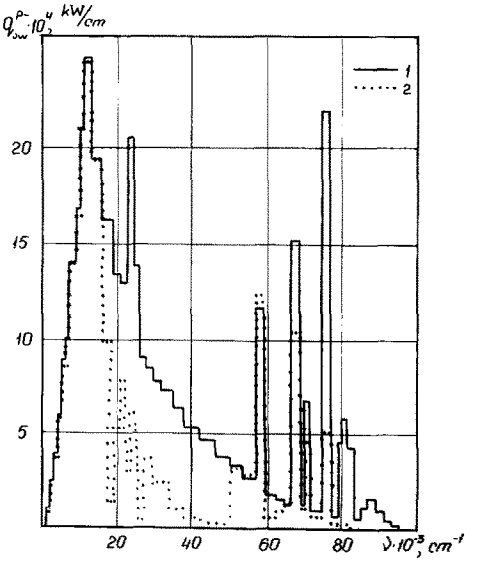

FIG. 7.

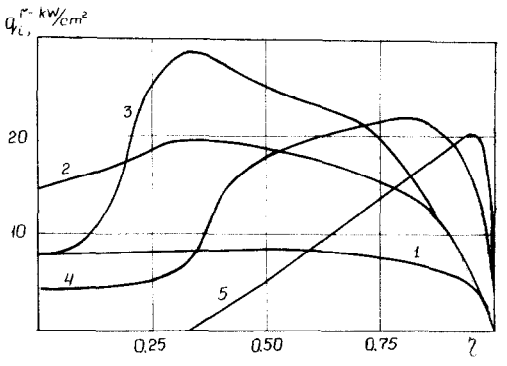

FIG. 8(a).

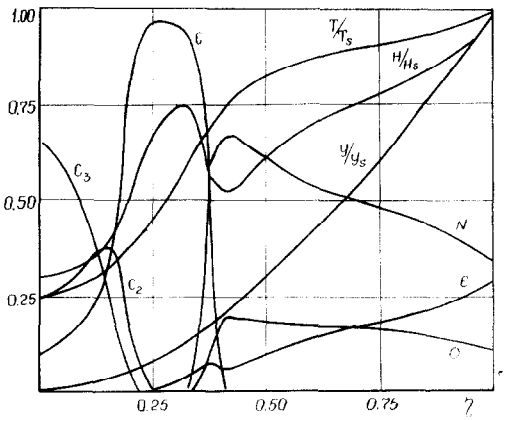

FIG. 8(b).

Attenuation of radiation within ranges 3 and 2 occurs in the region where the amount of graphite ablation products is substantial. Attention attaches to a clearly defined "hump" on the enthalpy profile. It originates due to dissociation of the molecules C_2 and C_3 as a result of radiation absorption. Moreover, ionization of the C atom occurs. This maximum of enthalpy gives rise to the mechanism of diffusive cooling of the layer of ablation products by diffusive heat conduction. Substantial temperature and concentration gradients in the layer of ablation products are responsible for heat conduction and diffusion exerting an appreciable effect on its structure. This may well be an explanation for the difference between the results of the present work and of [5] where the compressed layer was assumed to be non-conducting and no radiation attenuation was detected in the spectrum region $\nu < 60 \cdot 10^3\ \mathrm{cm}^{-1}$.

On the practical side, it is of great interest to determine the mass loss rate under steady-state conditions. Figure 9 shows dependence of f_w on the incident flow velocity. Curve 1 refers to $p = 1$ atm, $R = 1$ m; curve 2, to $p = 1$ atm, $R = 0{\cdot}3$ m; curve 3, $p = 1$ atm, $R = 3$ m; curve 4, $p = 0.3$ atm, $R = 1$ m; curve 5, $p = 3$ atm, $R = 1$ m and curve 6, $p = 10$ atm, $R =$

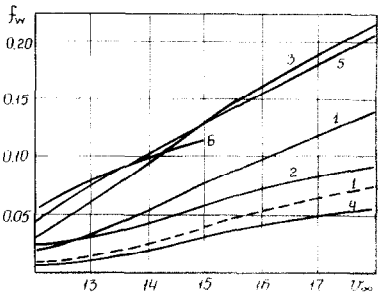

FIG. 9.

1 m. Dash-dotted curve 1 has been obtained from calculations where the continuum contribution alone was taken into account. It underestimates the mass loss rate by about a factor of two.

RADIATIVE-CONVECTIVE HEAT TRANSFER ON REFLECTING SURFACES

Radiation reflected from the surface re-enters the compressed layer where it becomes partially absorbed. The u.v. portion of the reflected radiation is absorbed in a relatively cold region of the compressed layer adjacent to the surface. This is due to photodissociation of molecular oxygen and photoionization of this and other molecules and also of atoms. The long-wave component can be absorbed only in a high-temperature region of the compressed layer as a result of free–bound and free–free transitions. Moreover, a certain effect can be exerted by line self-absorption. Absorption can bring about a rise in temperature and enthalpy in the outer portion of the compressed layer thus increasing its luminosity. Temperature and enthalpy gradients in the wall region should also become higher as well as the convective heat flux to the surface. The wall region will be less efficient in screening radiation in the vacuum u.v. region, which is also confirmed by the results of numerical calculations. Figures 10(a), 11(a) give the enthalpy profiles in a compressed layer. The variable η, introduced above, has been used as a coordinate. Also shown is the dependence of the physical coordinate y on η. Curves 1 (solid) refer to the reflection coefficient $r = 0$, curves 2 (dashed), to $r = 1$. Figure 10 shows the version with $V_\infty = 18$ km/s, $p = 1$ atm, $R = 1$ m, while Fig. 11, with $V_\infty = 15$ km/s, $p = 10$ atm, $R = 1$ m. In the first case, $y_{s1} = 3.2$ cm, $y_{s2} = 3.3$ cm, in the second case $y_{s1} = 3.7$ cm, $y_{s2} = 3.8$ cm. When $p = 1$ atm, it is seen that reflection causes a noticeable reduction of the thermal boundary layer thickness (gas layer where the effects of heat conduction are appreciable). At $p = 10$atm, a more pronounced feature is an increase in the enthalpy in that portion of the compressed layer where the temperatures are high and from which radiation originates. Figures 10(b) and 11(b) give distributions of Δq^r_{wi} for the components of radiative flux reflected from the surface in separate spectral ranges that have been introduced above. At $p = 1$ atm, absorption

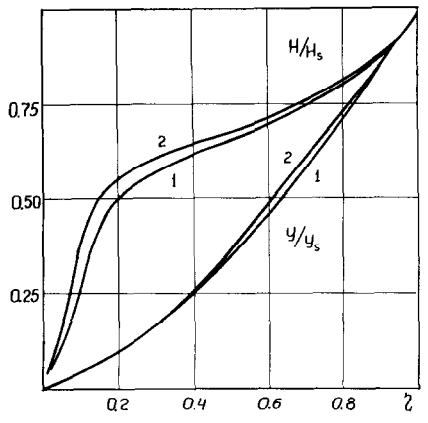

FIG. 10(a).

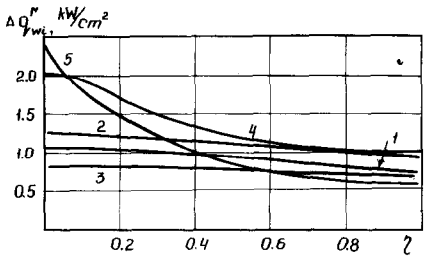

FIG. 10(b).

occurs mainly in ranges 4 and 5. Radiation in range 5 is absorbed for the most part in the region of the boundary layer. Absorption in range 4 occurs almost entirely due to line self-absorption. The coefficients k_ν for the continuum contribution are small in this range, but there are lines here which have strong reabsorption (self-absorption). The radiant energy Δq^r_{w4} is mostly absorbed in the high-temperature region of the compressed layer where the lower levels of corresponding transitions are populated.

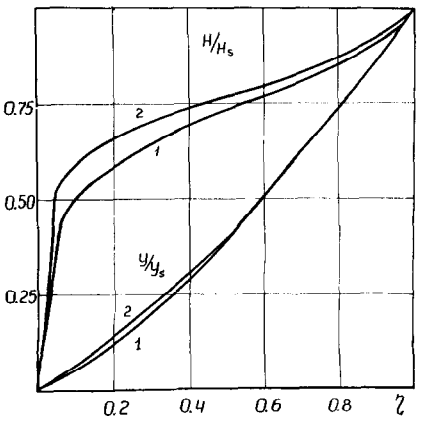

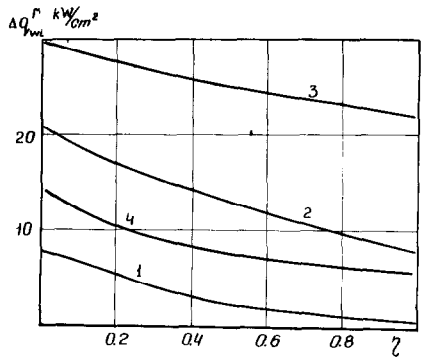

FIG. 11(a, b).

At $p = 10$ atm, the reflected radiation is absorbed in all spectral ranges and over the entire compressed layer. The boundary layer absorption does not play here any substantial role.

Quantitatively, an increase in radiative and convective fluxes to the surface, in the case when r is

Table 4. Heat fluxes to the surface and coefficients a^r and a^c at $r = 0$. Diffuse reflection. $T_w = 3000$ K

V_∞ (km/s)	p (atm)	R (m)	q^r_w (kW/cm²)	q^c_w (kW/cm²)	a^r	a^c
12	1	1	2.0	0.99	0.055	0.14
15	1	1	4.7	1.5	0.089	0.30
18	1	1	6.9	2.1	0.103	0.37
15	1	0.3	3.2	2.7	0.056	0.16
15	1	3	6.6	0.81	0.098	0.42
15	0.3	1	1.15	0.78	0.052	0.18
15	0.3	3	1.61	0.47	0.087	0.31
15	3	0.3	11.5	4.8	0.085	0.26
15	3	1	16.9	2.5	0.100	0.40
15	10	0.3	43.9	8.4	0.095	0.37
15	10	1	66.1	4.5	0.116	0.52

independent of ν, can be characterized by the coefficients a^r and a^c that can be determined from

$$q_w^r = q_{w(r=0)}^r (1 + r \cdot a^r),$$

$$q_w^c = q_{w(r=0)}^c (1 + r \cdot a^c).$$

The calculations show that actually a^r and a^c do not depend on r. Table 4 lists the predicted values of these coefficients for the conditions chosen.

It can be seen that a^r and a^c vary with the incident flow velocity. At V_∞ fixed, these coefficients increase with p and R. When the values of the combination $p \cdot R$ are close, so are the values of a^r and a^c. Similar behaviour can be observed also at other values of V_∞. This made it possible to derive generalized relationships for the coefficients of heat flux amplification in the form of functions of the complex $p \cdot R$. Figure 12 (a, b) presents approximation of the values of a^r and a^c obtained from numerical calculation with the use of the functions of the parameter $\log(p \cdot R)$. In this figure, 1 corresponds to $V_\infty = 12$ km/s; 2, $V_\infty = 15$ km/s; 3, $V_\infty = 18$ km/s. The quantity a^c has been approximated by linear relationship, while a^r, by quadratic paraboles. The deviations are less than 20%.

Calculations have been also carried out to estimate the effect of accounting for the reflection from real surfaces. Figure 13 shows the reflection coefficient for tungsten (curve 1) as a function of ν. The data on r_ν were taken from [21, 22]. This figure also contains r_ν's for a volumetrically reflecting heat shield based on especially pure silicon whose description is given elsewhere [23]. Of special interest is tungsten which has high values of r_ν in the vacuum u.v. region. The importance of accounting for absorption of the reflected radiation in the compressed layer can be characterized by the factor ε which shows the amount by which the heat flux calculated, taking into account the reflected radiation absorption, exceeds that obtained at $\Delta q_w^r = 0$.

Besides ε^r for q_w^r and ε^c for q_w^c we can consider ε^{in} which is the coefficient that describes an increase in the heat flux directed into the body, q_w^{in}. This heat flux is determined as

$$q_w^{in} = q_w^c + \int_0^{\infty} q_w^r (1 - r_\nu)\, d\nu - \varepsilon_w \sigma T_w^4.$$

It is by q_w^{in} that heating of the body is determined. Table 5 gives the values of ε for the extreme flow conditions.

For tungsten, the reflection was assumed to be specular and $T_w = 2000$ K, for silicon, to be diffuse and $T_w = 1500$ K. For the silicon coating at $p = 0.3$ and 1 atm the values of ε are very small and are therefore ignored.

Graphite ablation products seem by their properties to be media typical for other materials that can be used as protective coatings. This allows one to consider the effect of reflection on heat transfer with carbon vapour blowing as a model problem. Figure 14 shows the dependence of q_w^r (1) and q_w^c (2) on f_w at $V_\infty = 15$ km/s, $p = 10$ atm, $R = 1$ m. The statement of the problem is similar to that used for graphite. Dashed lines refer to $r = 0$, solid lines, to $r = 1$. It can be seen that in this case absorption of the reflected radiation affects q_w^c to a greater extent than in the absence of blowing. A complete blockage of the convective heat flux is detained. It is the effect of the convective heat flux which governs ablation of heat shields having high reflectivities. Thus, an increase in the convective heat flux in the presence of reflection should be allowed for when designing the heat shielding systems.

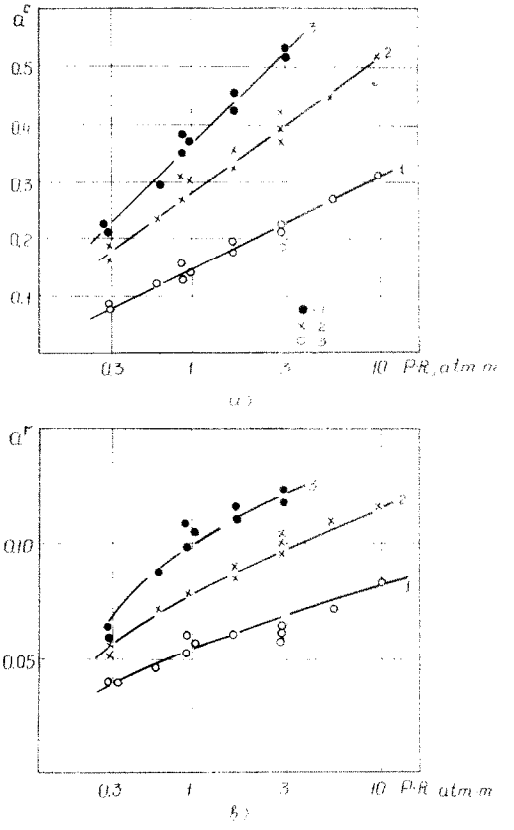

FIG. 12(a, b)

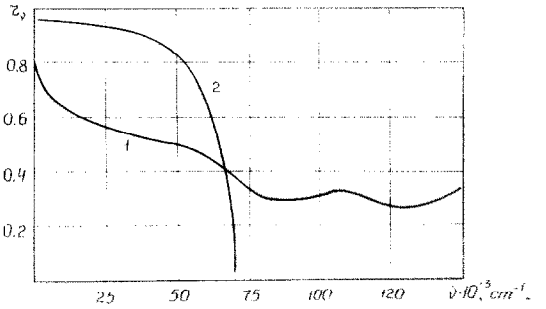

FIG. 13.

Table 5. Coefficients showing increase in heat fluxes to real surfaces

V_∞ (km/s)	p (atm)	R (m)	Tungsten ε^r (%)	Tungsten ε^c (%)	Tungsten ε^{in} (%)	Silicon ε^r (%)	Silicon ε^c (%)	Silicon ε^{in} (%)
18	1	3	4.4	15.2	7.5	3.7	11.2	3.6
18	3	1	4.8	17.4	8.1	4.4	10.0	8.0
18	0.3	3	3.6	11.4	6.4	—	—	—
18	1	1	3.6	12.0	7.4	—	—	—
15	10	1	5.2	19.8	8.7	7.0	13.0	11.4

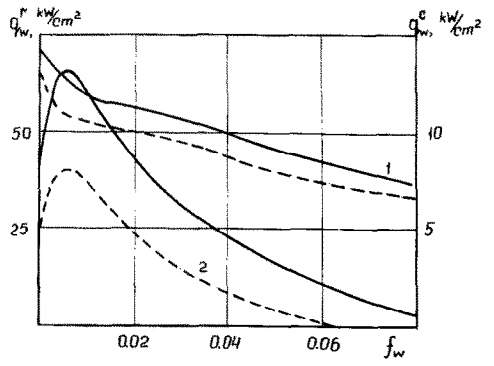

FIG. 14.

REFERENCES

1. L. M. Biberman, S. Ya. Bronin and A. N. Lagar'kov, Radiative-convective heat transfer of a blunt body in hypersonic flow, *Izv. Akad. Nauk SSSR*, Mekh. Zhid. Gaza No. 5, 112–123 (1972).
2. V. P. Zamuraev, I. I. Maslennikova and R. I. Soloukhin, Study of radiative heat transfer behind shock waves by multi-group averaging technique, in *Heat and Mass Transfer in Strong Radiative and Convective Heating*, Izd. ITMO AN BSSR, Minsk. pp. 3–18 (1977).
3. A. B. Karasyov and T. V. Kondranin, Some laws governing heat transfer in hypersonic shock layer in the presence of mass loss, *Izv. Akad. Nauk SSSR*, Mekh. Zhid. Gaza No. 3, 136–143 (1973).
4. A. B. Karasyov, T. V. Kondranin and I. N. Kuz'minsky, Some specific features of heat transfer in a chemically equilibrium boundary layer, *Izv. Akad. Nauk SSSR*, Mekh. Zhid. Gaza No. 4, 56–64 (1976).
5. L. M. Biberman, S. Ya. Bronin, M. V. Brykin and A. Kh. Mnatsakanyan, The effect of gaseous heat shield ablation products on heat transfer in the vicinity of the blunt body stagnation point, *Izv. Akad. Nauk SSSR*, Mekh. Zhid. Gaza No. 3, 129–136 (1978).
6. C. D. Engel, R. C. Farmer and R. W. Pike, Ablation and radiation coupled viscous hypersonic shock layers, *AIAA Jl* **11**(8), 1174–1184 (1973).
7. J. N. Moss, Radiative viscous shock-layer solution with coupled ablation injection, *AIAA Jl* **14**(9), 1311–1317 (1976).
8. K. M. Magomedov, Hypersonic flow of a viscous gas past blunt bodies, *Izv. Akad. Nauk SSSR*, Mekh. Zhid. Gaza No. 2, 45–56 (1970).
9. A. N. Rumynsky and V. P. Churkin, Hypersonic flow of a viscous radiating gas past blunt bodies, *Zh. Vychisl. mat. i mat. Fiz.* **14**(6), 1553–1570 (1974).
10. I. V. Avilova, L. M. Biberman, V. S. Vorobiyov, V. I. Zamalin, G. A. Kobzev, A. N. Lagar'kov, A. Kh. Mnatsakanyan and G. E. Norman, Optical properties of hot air, *Izd. Nauka, Moscow* (1970).
11. V. A. Kamenshchikov, Yu. A. Plastinin, V. M. Nikolaev and L. A. Novitsky, Radiative properties of gases at high temperatures, *Izd. Mashinostroenie, Moscow* (1971).
12. M. N. Rolin, R. I. Soloukhin and F. B. Yurevich, Effect of radiation reflection on radiative–convective heat transfer in hypersonic flow past blunt bodies, *Zh. Prikl. Mekh. Tekh.* No. 2, 99–107 (1980).
13. K. H. Wilson and W. E. Nicolet, Spectral absorption coefficients of carbon, nitrogen and oxygen atoms *J. Quant. Spectros. Radiat. Transfer* **7**(7), 841–972 (1967).
14. W. E. Nicolet, Users manual for the generalized radiation transfer code, *Aeroterm. Rep.* UM-69-9, USA (1969).
15. R. P. Main and E. Bauer, Equilibrium opacities and emissivities of hydrocarbon–air mixtures, *J. Quant. Spectros. Radiat. Transfer* **9**(4), 527–557 (1967).
16. O. N. Suslov and G. A. Tirsky, Determination of the properties and calculation of the effective ambipolar diffusion coefficients in a laminar multi-component boundary layer, *Zh. Prikl. Mekh. Tekh. Fiz.* No. 4, 60–72 (1970).
17. M. N. Rolin, F. B. Yurevich and V. V. Kondrashov, An approximate method for calculation of multi-component diffusion in high-temperature gas mixtures, in *High-Temperature Heat and Mass Transfer*, pp. 3–11. Izd. ITMO AN BSSR, Minsk (1975).
18. M. N. Rolin, F. B. Yurevich and V. V. Kondrashov, An approximate method for calculation of heat transfer coefficients of partially ionized gas mixtures, *J. Engng Phys.* **34**(3), 296–302 (1978).
19. M. N. Rolin and F. B. Yurevich, An economical approach to calculation of flows in the vicinity of stagnation point, in *Heat and Mass Transfer on Strong Radiative and Convective Heating*, pp. 33–43. Izd. ITMO AN BSSR, Minsk (1977).
20. Yu. V. Polezhaev and F. B. Yurevich, Heat Shielding, *Izd. Energiya, Moscow* (1976).
21. A. N. Ziidel and E. Ya. Shreider, *Vacuum Ultraviolet Spectroscopy*, Izd. Nauka, Moscow (1972).
22. I. K. Kikoin (Editor), *Tables of Physical Quantities*, Atomizdat, Moscow (1976).
23. J. C. Blome, D. N. Drennan and R. J. Schmitt, High-purity silica reflective heat shield, *Radiative Transfer and Heat Control*, pp. 131–152. New York (1976).

TRANSFERT DE CHALEUR ET DE MASSE DANS UNE COUCHE CPMPRIMEE ET EMETTRICE, AVEC UNE REFLEXION DEPUIS LA SURFACE DU CORPS ET DES PRODUITS INJECTES OU ABLATES

Résumé—On analyse le transfert thermique par rayonnement et convection pour un corps axisymetrique émoussé dans un écoulement d'air hypersonique. On présente les résultats du calcul des flux thermiques par rayonnement et par convection sur la surface de graphite en ablation. On dégage l'effet de réduction du transfert radiatif par rapport au flux radiatif calculé.

Une évaluation quantitative est faite de la tendance à l'accroissement des flux thermiques dirigés sur une surface réfléchissante à cause de l'absorption du rayonnement réfléchi dans la couche comprimée.

WÄRME- UND STOFFÜBERTRAGUNG IN EINER EMITTIERENDEN KOMPRIMIERTEN SCHICHT MIT REFLEXION VON DER KÖRPEROBERFLÄCHE UND INJEKTION VON ABLATIONSPRODUKTEN

Zusammenfassung—Dieser Aufsatz befaßt sich mit der Analyse des Wärmeübergangs durch Strahlung und Konvektion an einem stumpfen Körper, der sich in einer Überschall-Luftströmung befindet. Berechnungsergebnisse werden dargestellt, die sich für den auf eine verdampfende Graphit-Oberfläche gerichteten Wärmestrom infolge von Strahlung und Konvektion ergeben. Der Einfluß der Berücksichtigung des Strahlungswärmeaustausches wird aufgezeigt. Die Tendenz des auf eine reflektierende Oberfläche gerichteten Wärmestroms, durch Absorption von reflektierter Strahlung in einer komprimierten Schicht zuzunehmen, wird qualitativ abgeschätzt.

ТЕПЛО- И МАССООБМЕН В ИЗЛУЧАЮЩЕМ СЖАТОМ СЛОЕ ПРИ НАЛИЧИИ ОТРАЖЕНИЯ ОТ ПОВЕРХНОСТИ ТЕЛА И ВДУВА ПРОДУКТОВ РАЗРУШЕНИЯ

Аннотация — Рассматривается радиационно-конвективный теплообмен при обтекании осесимметричного затупленного тела гиперзвуковым потоком воздуха. Приводятся результаты расчетов радиационного и конвективного тепловых потоков к поверхности разрушающегося графита. Показано влияние учета переноса излучения на расчетные значения радиационного теплового потока.

Проведена количественная оценка эффекта увеличения тепловых потоков к поверхности, обладающей отражением, в результате поглощения отраженного излучения в сжатом слое.